PAPER

Check for updates

From waste to precious: recovering and anchoring Au from electronic wastewater onto poly(*m*-phenylenediamine) membranes for catalytic nitrophenol conversion†

Youmei Xu,‡[a] Yuchao Chen,‡[a] Mengxia Wang,[ab] Yufei Shu,[a] Siyu Cao[a] and Zhongying Wang 🆔 *[ac]

Nitrophenol wastewater treatment and extracting and reusing precious metals from electronic wastewater have recently gained considerable attention. In this study, polyaniline-based membranes showcased remarkable gold recovery capability from electronic wastewater, effectively reclaiming 100% of gold on the membrane surface even in the presence of competing metal cations. The prepared Au@PmPD membrane, characterized by its high specific surface area and abundant Au nanoparticles (NPs), demonstrated excellent catalytic activity and stability, maintaining near 100% conversion efficiency in reducing 4-NP to 4-AP in the presence of $NaBH_4$ over extended durations. Compared with the conventional physical mixing method, our *in situ* formation of the Au@PmPD membrane highlights the superior distribution of Au NPs and active sites for enhanced catalytic efficiency. It eliminates the need for additional steps to load Au NPs onto the membrane, resulting in a more straightforward and efficient process. Overall, this research provides a sustainable approach to repurposing waste into precious resources and offers a promising solution for the efficient treatment of persistent organic pollutants in wastewater, aligning with the principles of a circular economy.

Environmental significance

This study highlights the environmental significance of utilizing Au@PmPD membranes for the dual purpose of recovering valuable gold from electronic waste and catalytically reducing hazardous 4-nitrophenol in wastewater. By achieving 100% gold recovery and demonstrating robust catalytic performance in degrading persistent organic pollutants, the membrane technology presents a sustainable approach to waste management. It not only mitigates the environmental impact of e-waste and industrial wastewater but also contributes to resource recovery and pollution reduction, aligning with the goals of a circular economy and cleaner production.

Introduction

Nitrophenols are a group of organic compounds characterized by the presence of one or more nitro groups (–NO₂) attached to a phenol ring. These compounds find extensive applications across various anthropogenic activities, including the production of pesticides, dyes, and explosives.[1–3] Widely acknowledged as toxic substances, nitrophenols pose significant threats to both human health and the natural environment. Human ingestion of nitrophenols has been documented to cause

[a]School of Environmental Science and Engineering, Southern University of Science and Technology, Shenzhen 518055, China. E-mail: wangzy6@sustech.edu.cn

[b]School of Environment, Harbin Institute of Technology, Harbin 150001, China

[c]Guangdong Provincial Key Laboratory of Soil and Groundwater Pollution Control, Southern University of Science and Technology, Shenzhen 518055, China

† Electronic supplementary information (ESI) available: Concentration–absorbance standard curve of 4-NP (Fig. S1); XRD pattern of PmPD nanoparticles (Fig. S2); plot of zeta potential *versus* pH for cross-linked PmPD (Fig. S3); C, N elemental mapping spectra of the Au@PmPD membrane (Fig. S4); high-resolution N 1s XPS spectra of the PmPD membrane before and after Au(III) recovery (Fig. S5); N₂ adsorption–desorption isotherm of Au@PmPD (Fig. S6); UV-vis absorbance changes of 4-NP before and after passing through the Au@PmPD membrane (Fig. S7); color change of 4-NP solution before and after the catalytic reduction reaction through the Au@PmPD membrane (Fig. S8); the effect of PmPD loading on the catalytic performance of the Au@PmPD membrane (Fig. S9); SEM-EDS mapping spectra of the Au@PmPD membrane after a 136-min reaction (Fig. S10); plot of flux and residence time *versus* pressure for the Au@PmPD membrane (Fig. S11); size distribution of Au NP dispersion (Fig. S12); the measurement of effective pore volume (Text S1); comparison of catalytic reduction of 4-NP by the Au@PmPD membrane with that by the membranes reported in the published literature (Table S1); characteristics of simulated electronic wastewater (Table S2); quality characteristics of simulated dyeing wastewater (Table S3). See DOI: https://doi.org/10.1039/d4va00010b

‡ The authors contributed equally to the work.

detrimental effects on the body, such as the liver, kidney, and central nervous system.[4] Moreover, they possess mutagenic and carcinogenic properties, elevating the risk of cancer development in exposed individuals.[5] Beyond the direct implications for human health, nitrophenols also impose adverse consequences on the environment. Due to their persistent nature in the environment,[6] these compounds tend to accumulate in soil and aquatic ecosystems, thereby endangering the health of aquatic life and other organisms due to the toxic impact of nitrophenols.[7]

Various methods are available for removing nitrophenols from contaminated water sources. Commonly employed approaches include advanced oxidation processes (AOPs),[8] the adsorption method,[8,9] and electrochemical treatment.[10] Among these, catalysis emerges as a preferred choice owing to its efficiency and environmentally friendly characteristics.[11,12] It eliminates the necessity for harsh chemicals and high energy consumption, making it a more sustainable and practical option. However, nanoparticle catalysts tend to aggregate, necessitating support structures to enhance their specific surface area and active sites. Recent advancements have spotlighted catalysis facilitated by membranes, drawing attention to its straightforward application and the potent synergistic benefits it accrues from combining membrane processes with catalytic action.[13,14] Moreover, the catalytic membrane not only retains the advantages of traditional catalysis, but also allows for easy regeneration and reuse, thereby further enhancing its practicality. In membrane catalysis for nitrophenols, sodium borohydride ($NaBH_4$) is commonly employed as a reducing agent. As wastewater containing nitrophenols passes through the membrane, nitrophenol molecules and $NaBH_4$ interact with the catalyst impregnated within the membrane, prompting the reduction of the nitro group ($-NO_2$) to an amino group ($-NH_2$). For example, Yu et al. developed a porous wood membrane decorated with gold nanoparticles (Au NPs), capable of continuously converting over 98% of 4-nitrophenol (4-NP) to 4-aminophenol (4-AP) at a reaction constant of 0.152 min^{-1} with $NaBH_4$.[15] Similarly, Fang et al. prepared an ultrafiltration membrane loaded with Ag NPs within its inner pores to separate and catalyze the degradation of pollutants, achieving a 98.0% conversion of 4-NP with $NaBH_4$ even in the presence of humic acid.[16]

Presently, the application of membrane catalysis for nitrophenol removal faces several limitations. The catalyst predominantly consists of expensive precious metal nanoparticles,[17,18] such as gold (Au), and the cost associated with integrating Au NPs into the membrane can be prohibitive. This high expense may impede the scalability of the method and limit its practicality for large-scale treatment applications. Additionally, conventional membrane substrates, such as polyvinylidene fluoride (PVDF)[19] and carbon nanotubes (CNTs),[20] lack specific interactions with Au, leading to a limited loading capacity of Au NPs within the membrane. Such a low loading capacity typically implies a scarcity of catalytic sites, thereby diminishing the overall effectiveness of the nitrophenol removal process. Furthermore, the weak interaction between Au and membrane substrates may pose the risk of Au NP leaching into the treated

water, potentially causing secondary environmental contamination, as well as a decline in the catalytic activity of the membrane over time.

Electronic waste (e-waste) is rich in precious metals such as Au and can be a potential source for Au-laden catalytic membranes.[21,22] It has emerged as the fastest-growing component of urban solid waste, with annual global production ranging from 20 to 50 million tons,[23] prompting widespread societal concern. The significant economic and environmental value associated with the Au content found in e-waste, which is often several times greater than that found in native gold ore,[24,25] underscores the importance of developing comprehensive technologies for the efficient, cost-effective, and environmentally friendly recovery of Au from e-waste. However, the complexity of e-waste coupled with the relatively low concentration of Au compared to other metals poses challenges to the effective recovery of pure Au.[26] Currently proposed hydrometallurgical approaches for Au recovery from e-waste primarily involve three steps: pretreatment, Au leaching, and subsequent separation and recovery.[27] The most widely used leaching methods in industry involve strongly corrosive and toxic aqua regia and cyanidation, which produce a large amount of electronic wastewater and pose serious environmental risks.[28,29] Additionally, these processes entail additional steps for desorption and separation of the Au complex with a leaching agent, thereby increasing investment costs. In this context, e-waste represents both a significant challenge and a valuable opportunity as a potential source for Au-laden catalytic membranes, which could address the critical need for pollutant degradation and resource recovery.

To address these dual challenges, we propose an innovative strategy that involves the engineering of a specialized membrane with an enhanced affinity for Au, intending to utilize it for anchoring Au from electronic wastewater, particularly e-waste leaching solutions known to contain substantial concentrations of precious metals. By selectively extracting Au from these solutions and affixing it onto the membranes as a catalyst, we aim to reduce the overall costs while also contributing to resource recycling efforts. To achieve this, the membrane surface will incorporate chemical binding sites such as amines, amides, and other relevant groups that are known for their strong affinity for Au.[30–32] Furthermore, this particular membrane is expected to possess essential properties, including corrosion resistance, structural durability, and chemical stability, which are crucial for maintaining prolonged and effective catalytic performance.[33] To the best of our knowledge, a functionalized membrane capable of extracting Au from electronic wastewater while possessing high catalytic performance for nitrophenol conversion is currently absent from the existing research landscape.

In this study, poly(m-phenylenediamine) (PmPD) membranes were employed to extract Au and serve as catalytic membranes for nitrophenol conversion. The selection of the PmPD membrane was based on its surface rich in amino groups, enhancing the affinity for Au, and its inherent chemical stability. The PmPD membrane was prepared through an oxidative polymerization method, and Au NPs were

immobilized onto the membrane surface by *in situ* sorption to decrease their agglomeration effect. For the nitrophenol conversion experiment, 4-nitrophenol (4-NP) was selected as a model contaminant. The catalytic activity of the Au@PmPD membrane for 4-NP reduction was evaluated through membrane catalysis experiments. Various parameters, such as PmPD and Au loadings, the addition of the reducing agent, pH, and co-existing anions, were systematically investigated to assess their influence on the 4-NP reduction efficiency. Additionally, the stability and reusability of the Au@PmPD membrane were evaluated to ascertain its long-term viability in nitrophenol reduction applications. This research aims to develop a novel functionalized Au@PmPD membrane by *in situ* recovery of gold from electronic wastewater and utilizing it for nitrophenol removal through catalytic reduction. This approach presents a potential strategy for repurposing precious metals from e-waste, thereby contributing to a circular economy.

Materials and methods

Materials and chemicals

Chloroauric acid (HAuCl$_4$, 48–50% for Au) was purchased from Macklin, China, and 4-nitrophenol (4-NP, 98%) was obtained from Aladdin, China. *m*-Phenylenediamine (MPD, 99%, Aldrich), cupric chloride dihydrate (CuCl$_2$·2H$_2$O, Macklin, China), sodium periodate (NaIO$_4$, 99.5%, Macklin, China), and glutaraldehyde (GA, 50% in water, Aladdin, China) were used to prepare the PmPD nanoparticles and membranes. Sodium borohydride (NaBH$_4$, 98%, Aladdin, China) was used for the reductive conversion of 4-NP. Sodium citrate (99%, Macklin, China) was used to synthesize gold nanoparticles. Methylene blue (MB, 98%, Macklin, China) was used to simulate dyeing wastewater. All reagents used in this work were of analytical grade without further purification. Ultrapure water generated using a Millipore system (Millipore, Billerica, MA) was used for the preparation of all solutions.

Preparation of the PmPD membrane and Au loading

The fabrication process of the PmPD membrane commenced with the synthesis of PmPD nanoparticles, followed by their assembly into a membrane through cross-linking and vacuum filtration processes, as illustrated in Fig. 1. PmPD nanoparticles were synthesized through a polymerization process based on previous studies.[34,35] Initially, 2.0 g of MPD monomer and 1.26 g of CuCl$_2$·2H$_2$O were dissolved in 80 mL of ultrapure water, and then mixed with 100 g L^{-1} NaIO$_4$ as the oxidizing agent to initiate the polymerization process. The mixture was stirred in a homemade reactor at room temperature for 2 hours. The resulting PmPD nanoparticles were separated by centrifugation at 5000 rpm, followed by a series of washes with ultrapure water to eliminate excess oxidants and impurities. The purified nanoparticles were then redispersed in ultrapure water using an ultrasonic bath (SB25-12DTD, Ningbo Xinzhi Biotechnology Co., Ltd, China) to obtain a PmPD dispersion. To enhance the interaction between PmPD nanoparticles and ensure the structural stability of the PmPD membrane, the PmPD nanoparticles were cross-linked with 4 wt% of GA for 30 min at 60 °C in an oven. Subsequently, 15 mg of cross-linked PmPD nanoparticle dispersion was then loaded onto a nylon membrane (with a nominal pore size of 200 nm, Tianjin Jinteng Technology Co., Ltd) by vacuum filtration to obtain the PmPD membrane.

Au loading onto the PmPD membrane was conducted in a Millipore cell (UFSC40001, MilliporeSigma, U.S.A.) with a 4.0 cm diameter and a surface area of 12.56 cm^2. To simulate the Au species obtained from aqua regia etching solution, a HAuCl$_4$ solution was used as the source of Au-containing wastewater. For the capture and loading of Au, the PmPD membrane, containing 15 mg of PmPD nanoparticles at pH ~5.0, was filtered with 100 mL of HAuCl$_4$ solution containing 40 mg L^{-1} Au, under a 0.2 bar pressure as the driving force for 30 min. Throughout this process, the concentration of residual Au in the filtrate was monitored by inductively coupled plasma-optical emission spectrometry (ICP-OES; iCAP 7000 Series, Thermo Fisher Scientific, MA, U.S.A.). Notably, no Au ions were detected in the filtrate, indicating the successful immobilization of nearly all Au ions (amounting to 4.0 mg) into the PmPD adsorptive membrane. The resulting Au-laden PmPD membrane, referred to as Au@PmPD, was subsequently employed for the catalytic reduction of 4-NP.

Characterization

Scanning electron microscopy (SEM; Merlin, ZEISS, MA, U.S.A.) and transmission electron microscopy (TEM; Talos F200X, MA,
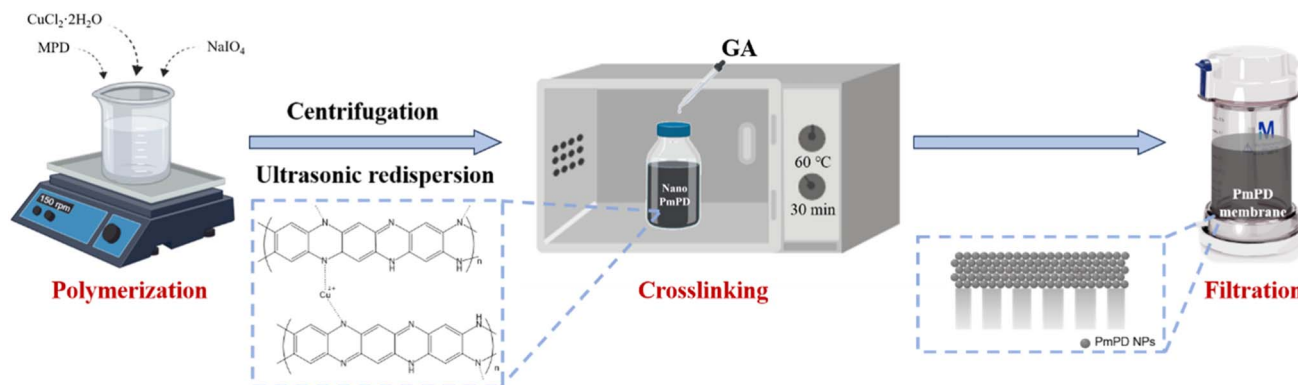

Fig. 1 Schematic representation of the PmPD membrane fabrication process.

U.S.A.) coupled with an energy-dispersive spectroscope (EDS) were employed to observe the morphology and surface structure of PmPD and Au@PmPD. Fourier-transform infrared spectroscopy (FT-IR; Vertex 70v, Bruker, Germany) was employed to identify the characteristic functional groups of PmPD. To further analyze the molecular structure of PmPD, Raman spectroscopy was performed on a LabRAM HR Evolution (HORIBA, Kyoto, Japan). X-ray diffraction (XRD; Rigaku Smartlab 9 kW, Tokyo, Japan) was used to determine the crystalline nature and compositions of the Au species deposited on PmPD. X-ray photoelectron spectroscopy (XPS; PHI 5000 Versaprobe III, ULVAC-PHI, Japan) was employed to measure the chemical compositions and oxidation states of PmPD before and after loading Au. Additionally, the N_2 adsorption–desorption isotherms were measured by Brunauer–Emmet–Teller analysis (BET; ASAP 2020, Micromeritics, U.S.A.) to analyze the specific surface area and pore size of Au@PmPD.

Catalytic reduction of 4-NP

The catalytic performance of the Au@PmPD membrane was evaluated through the reduction of 4-NP to 4-AP in the presence of $NaBH_4$ at room temperature. The catalytic reduction of 4-NP was conducted in a Millipore cell unit, with 100 mL solution containing 20 mg L^{-1} 4-NP and 25 mM $NaBH_4$ as the feed solution. The feed solution was filtered through the Au@PmPD membrane driven under various external pressures ranging from 0.2 to 2.6 bar in a single-pass mode without any recirculation. The catalytic conversion of 4-NP to 4-AP was monitored using a UV-vis spectrophotometer (UH5300, Hitachi, Japan), and the absorbance at specific wavelengths, such as 400 nm for

4-NP and 300 nm for 4-AP, in the UV-vis spectra was correlated with their concentrations in the permeate solutions (Fig. S1†). The efficiency of 4-NP conversion (η) by the Au@PmPD membrane was calculated using the following equation: $\eta = (1 - C_t/C_0) \times 100\%$, where C_0 and C_t represent the concentrations of 4-NP in the feed and permeate solutions, respectively. The conversion reaction was fitted with first-order kinetics, enabling the calculation of the apparent reaction rate constant (k_{obs}) using the equation $\ln(C_t/C_0) = -k_{obs} \times t$, where t denotes the residence time of the 4-NP molecule within the membrane.

Results and discussion

PmPD synthesis and characterization

PmPD nanoparticles were synthesized *via* the oxidative polymerization of MPD monomers, using $NaIO_4$ as the oxidizing agent and Cu ions as the complex metal to crucially facilitate electron transfer. This process initiated the creation of radical cations and subsequent polymer chain growth, leading to the formation of PmPD nanoparticles. These nanoparticles exhibited an amorphous nature, as evidenced by the absence of diffraction peaks in the XRD pattern (Fig. S2†). The morphology of the as-prepared PmPD nanoparticles was revealed by SEM (Fig. 2a) and TEM (Fig. 2b) imaging. These images depicted PmPD nanoparticles clustered in small spherical aggregates with diameters spanning tens of nanometers. FT-IR (Fig. 2c) was employed to reveal the molecular structure of PmPD. The broad absorption centered between 3600 and 3000 cm^{-1} implied the stretching mode of the –NH– group. Additionally, two distinct sharp peaks, located at ~1620 cm^{-1} and ~1500 cm^{-1}, corresponded to the stretching vibrations of quinoid imine (–C=N–)
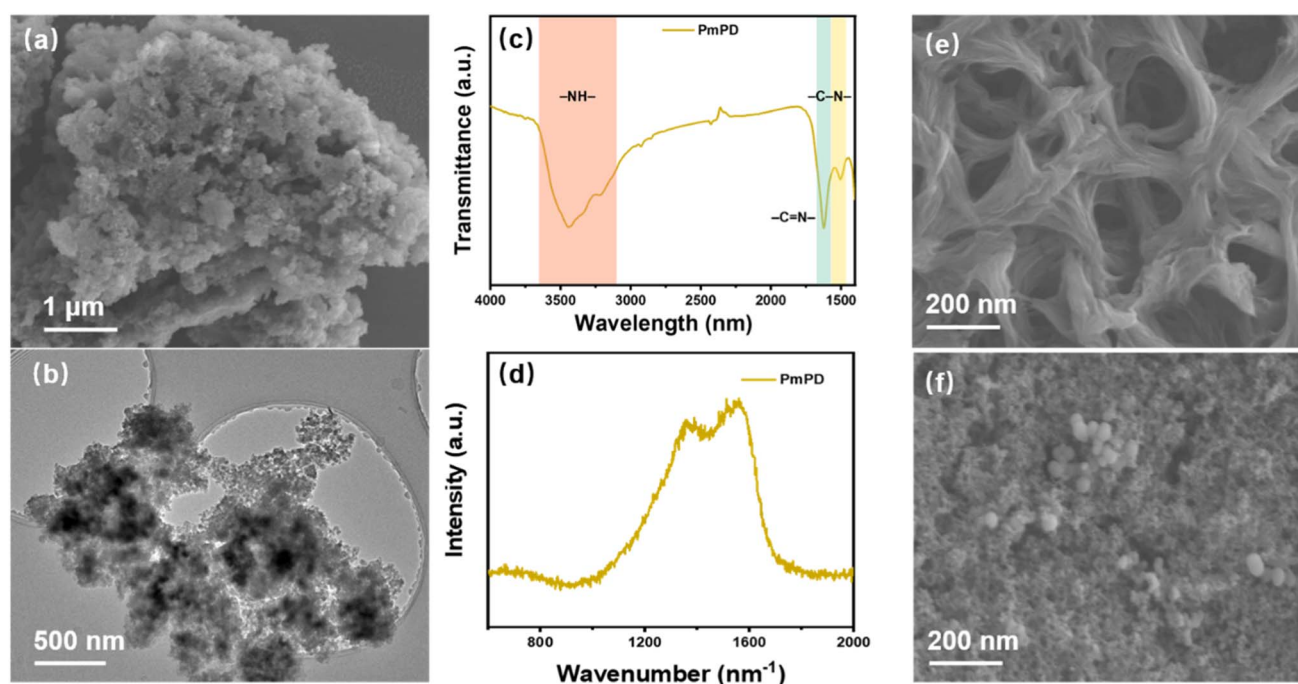

Fig. 2 Characterization of PmPD nanoparticles and membranes: (a) SEM image, (b) TEM image, (c) FT-IR spectra, and (d) Raman spectra of PmPD nanoparticles. SEM images of (e) nylon membrane substrate and (f) PmPD membrane.

and benzenoid amine (–C–N–) structures, respectively. In Raman spectra, the peak observed at ∼1573 cm^{-1} was attributed to the presence of quinoid structures, while the two peaks observed at ∼1330 and ∼1410 cm^{-1} were associated with the phenazine structure (Fig. 2d). The resulting PmPD nanoparticles were further processed into membranes through crosslinking and vacuum filtration onto a nylon membrane substrate. The surface morphology of both the nylon membrane and PmPD membrane was examined by SEM (Fig. 2e and f). The nylon membrane displayed a porous surface with an average pore size of ∼200 nm, while the PmPD membrane consisted of a dense layer of PmPD nanoparticles on top of the nylon substrate, significantly decreasing the apparent pore size of the membrane.

Au capture by the PmPD membrane

Au was successfully captured from the solution by the PmPD membrane in a single-pass mode without recirculation. Following the filtration of 100 mL of 40 mg L^{-1} Au solution using the PmPD membrane, the concentration of Au in the filtrate consistently remained undetectable, indicating the remarkable affinity and complete binding capability of PmPD for Au ions. This strong affinity is largely attributed to the abundant amino groups present within the PmPD membrane, enabling effective interaction with Au(III) ions through coordination. In addition, the positively charged PmPD membrane is capable of attracting and capturing AuCl$_4^-$ species, which is the dominant one in the aqua regia etching solutions of Au, via electrostatic interactions (Fig. S3†), further enhancing the adsorption and subsequent retention of Au ions within the PmPD membrane.

Following the loading of Au, both the structure and chemical composition of the Au@PmPD membrane were thoroughly characterized. SEM (Fig. S4a and b†) and TEM imaging (Fig. 3a) unveil the presence of distinct nanoparticles attached to PmPD particles. To examine the elemental distribution within Au@PmPD, EDS mapping was performed, revealing the uniform dispersion of the newly formed nanoparticles enriched with Au (Fig. 3b and c), along with other elements such as C and N (Fig. S4c and d†) across the entire PmPD surface. The average particle size of Au NPs was found to be ∼40 nm (as inserted in Fig. 3c). Further insight into the chemical composition of the Au@PmPD membrane was obtained through XRD and XPS measurements. The XRD pattern of the Au@PmPD membrane showcases the peaks observed at 38.28°, 44.5°, 67.74°, and 77.76° (Fig. 3d), corresponding to the (111), (200), (220), and (311) crystal planes of metallic Au, respectively. This
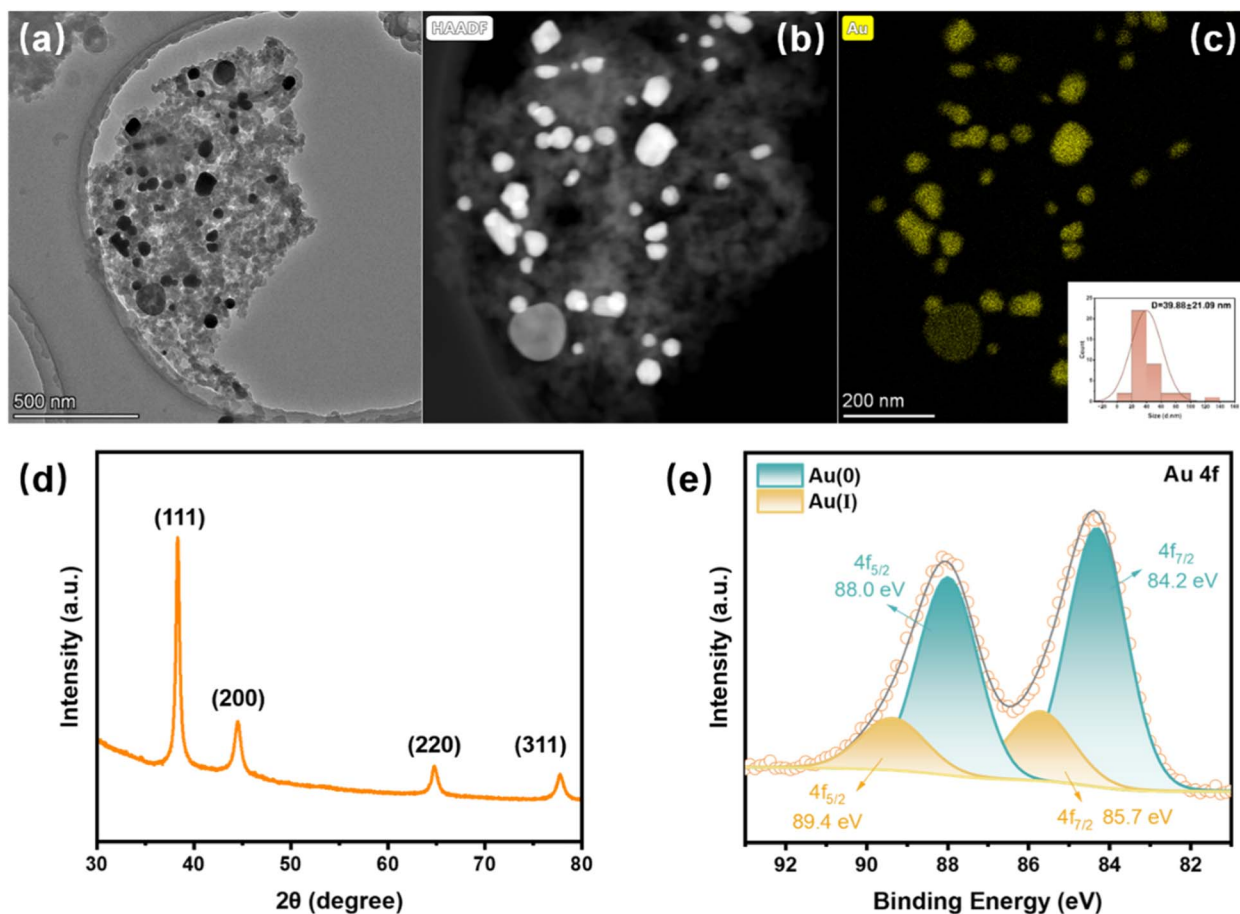

Fig. 3 Characterization of the Au@PmPD membrane: (a) TEM image, (b and c) TEM and EDS spectra showing the Au elemental mapping, (d) XRD pattern, and (e) high-resolution XPS spectra of Au 4f.

observation demonstrates the formation of Au nanoparticles within the PmPD membrane during the Au capture process. The Au 4f XPS spectra (Fig. 3e) revealed peaks at 84.2 and 88.0 eV, assigned to Au $4f_{7/2}$ and Au $4f_{5/2}$ of Au(0), respectively, as well as peaks at 85.7 and 89.4 eV attributed to Au $4f_{7/2}$ and Au $4f_{5/2}$ of Au(I), respectively. These findings confirm the presence of both Au(0) and intermediate Au(I) states, signifying the reduction of Au(III) on the surface of PmPD.

To elucidate the role of PmPD in the adsorption and reduction of Au(III), XPS characterization was performed on the PmPD membrane before and after Au(III) capture (Fig. S5†). The N 1s XPS spectra of the PmPD membrane (Fig. S5b†) display peaks at 397.9, 398.9, 399.7, and 400.4 eV associated with –NH– in the benzenoid amine units, –N=C– in both quinoid imine and phenazine, –N–C–, and –N$^+$=, respectively. A comparative analysis of the N 1s spectra before and after Au recovery indicates a noticeable shift towards higher binding energy following Au adsorption. Specifically, deconvolution analysis showed a decrease in the content of –NH– and –N=C– groups and an increase in the –N–C– group, confirming the interaction between gold and the functional groups (e.g., –NH–) in the PmPD membrane, corroborating the reduction of gold by these amino moieties.

Catalytic performance of the Au@PmPD membrane

The Au@PmPD membrane, distinguished by its high specific surface area (Fig. S6†) and abundant Au nanoparticles, offers a considerable number of active sites and catalytic reaction centers. Herein, the catalytic performance of the Au@PmPD membrane was examined in the catalytic reduction of 4-NP to 4-AP, employing NaBH$_4$ as a reducing agent. The conversion progress was monitored by observing the changes in the UV-vis absorbance at wavelengths of 400 and 300 nm, indicative of 4-NP and 4-AP concentrations, respectively. Upon filtration of 4-NP alone through the Au@PmPD membrane, minimal alteration in the absorbance of 4-NP was observed (Fig. S7†), indicating the membrane's inability to degrade 4-NP independently. Moreover, in the absence of the catalyst, NaBH$_4$ exhibited negligible degradation of 4-NP, as shown in Fig. 4. However, with the simultaneous exposure to both the Au@PmPD membrane and NaBH$_4$ by filtering the 4-NP and NaBH$_4$ mixture, the UV-vis absorbance of 4-NP in the filtrate at 400 nm almost disappeared, accompanied by the emergence of a new peak at 300 nm for 4-AP, affirming the catalytic reductive conversion from 4-NP to 4-AP (Fig. 4). Meanwhile, the color of the 4-NP feed solution changed from bright yellow to colorless in the filtrate (Fig. S8†). The PmPD membrane also accounted for ~57% of 4-NP removal, attributed largely to its superior adsorption retention ability. These findings unequivocally demonstrate the pivotal roles played by the Au@PmPD catalytic membrane and the NaBH$_4$ reducing agent in the 4-NP reduction.

To investigate the effects of PmPD and Au loadings on the catalytic reduction performance of 4-NP by the membranes, experiments were conducted with varying PmPD contents (5, 15, and 20 mg) and Au loadings (0.5, 1.0, 2.0, and 4.0 mg). As shown in Fig. S9,† different PmPD amounts in the membranes yielded
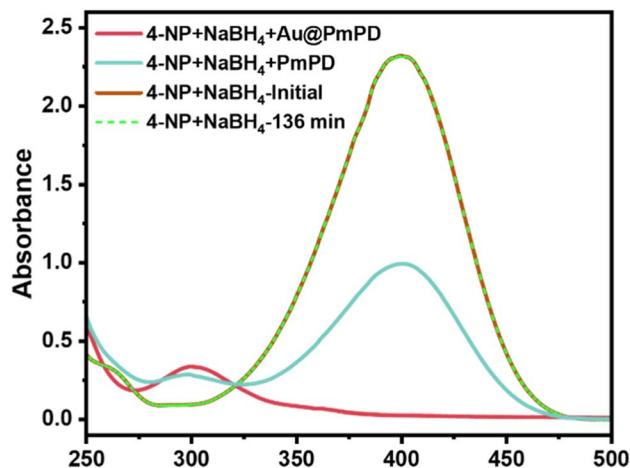

Fig. 4 UV-vis absorbance changes of 4-NP with NaBH$_4$ under different conditions: before and after 136 min and after the mixed solution passes through the PmPD and Au@PmPD membrane.

similar outcomes, suggesting that 5 mg of PmPD was sufficient to capture and reduce 4.0 mg Au(III) to Au NPs and to serve as the catalytic membrane for converting 4-NP. Fig. 5a shows that 1.0, 2.0, and 4.0 mg of Au NPs achieved nearly complete degradation of 4-NP, with higher loading of Au NPs correlating with an increased conversion rate from 4-NP to 4-AP. The concentration of NaBH$_4$, as the reducing agent, plays an important role in determining the reduction rate during the reduction process. Fig. 5b demonstrates that when the concentration of NaBH$_4$ reached 25 mM, the conversion efficiency of 4-NP reached nearly 100%.

To assess the impact of co-existing anions commonly found in industrial wastewater on the catalytic reduction of 4-NP using the Au@PmPD membrane, experiments were conducted with a mixture containing 20 mg L^{-1} 4-NP and the same mass concentration of NO$_3^-$, SO$_4^{2-}$, and PO$_4^{3-}$. The concentrations of these co-existing anions were monitored in the filtrate. The results demonstrated that the Au@PmPD membrane exhibited approximately 40% removal of PO$_4^{3-}$, while showing a minimal impact on the removal of NO$_3^-$ and SO$_4^{2-}$ (Fig. 5c). The slight removal of PO$_4^{3-}$ was likely caused by the electrostatic attraction between positively charged PmPD and the PO$_4^{3-}$ anion. However, the adsorption of PO$_4^{3-}$ did not compromise the catalytic conversion efficiency of 4-NP by the Au@PmPD membrane. The conversion efficiency of 4-NP by the Au@PmPD membrane remained nearly 100% throughout an 18-min duration, irrespective of the presence of co-existing anions. These results suggest that the presence of the anions had no significant effect on the conversion of 4-NP. The impact of initial pH on catalytic performance was investigated across a wide pH range from 3 to 11. Notably, it was found that pH had a minimal effect on the catalytic reduction, and the conversion efficiency of 4-NP maintained ~100% under all tested pH conditions (Fig. 5d). These results collectively underscore the Au@PmPD membrane's robustness and its potential applicability in effectively treating 4-NP in diverse wastewater environments.
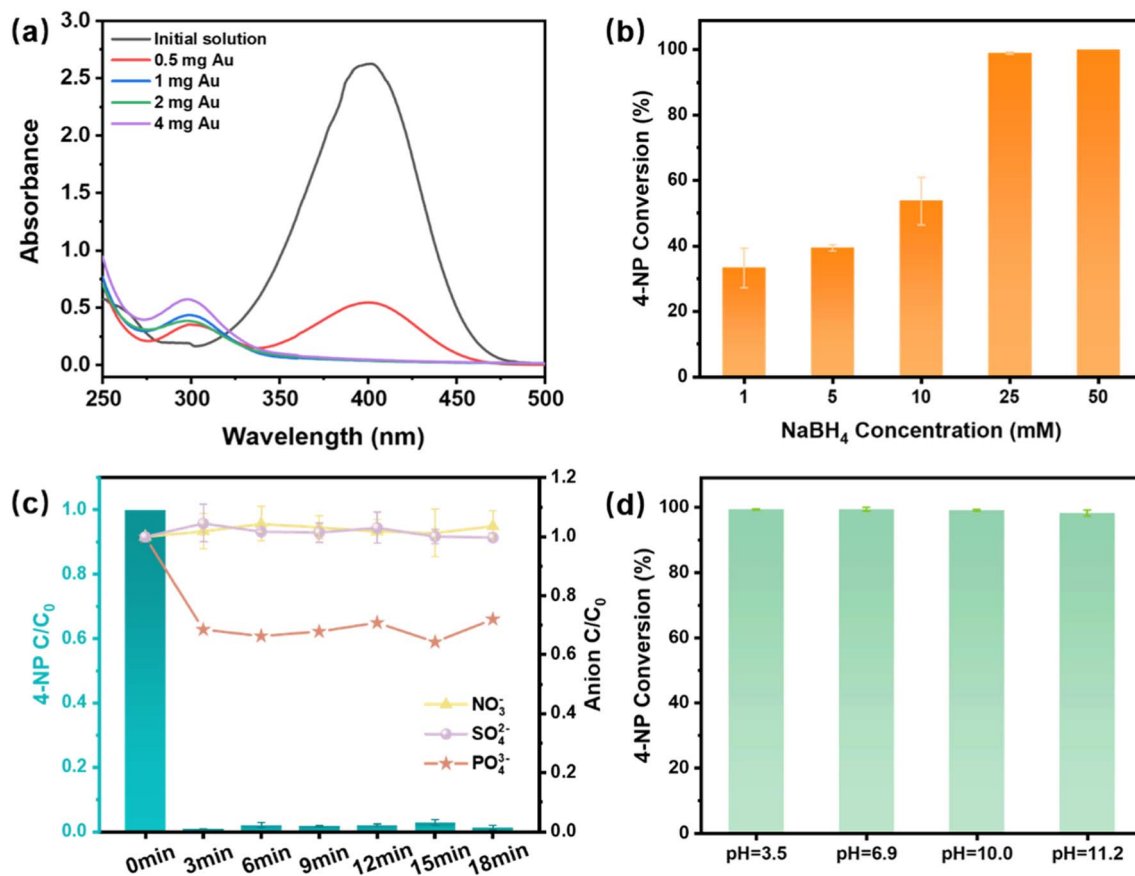
Fig. 5 Effects of different factors on the catalytic conversion performance of 4-NP by the Au@PmPD membrane in the single-pass filtration: (a) Au loading, (b) concentration of NaBH$_4$, (c) co-existing anions, and (d) pH of the 4-NP solutions.

To evaluate the long-term catalytic stability of the Au@PmPD membrane, an extended experiment spanning 136 minutes was conducted. Notably, the absorbance of 4-NP almost disappeared, and the catalytic reduction conversion efficiency remained remarkably stable, maintaining a near 100% conversion without any evidence of Au leaching throughout the entire duration (Fig. 6a and b). Several characterization studies were performed to further assess the changes in the morphology and compositions of the Au@PmPD membrane after the 136-min reaction. SEM-EDS (Fig. 6c and S10†) showed that the morphology of the used Au@PmPD membrane remained largely unchanged, with Au NPs consistently present on the surface of the membrane without apparent loss. Moreover, XRD (Fig. 6d), FT-IR (Fig. 6e), and XPS (Fig. 6f) reveal no significant shifts in peak positions or the emergence of new peaks. These results collectively affirm the Au@PmPD membrane's enduring catalytic capability in converting 4-NP to 4-AP and its substantial chemical stability over extended experimental duration, highlighting its robustness and suitability for long-term applications in catalytic processes.

The influence of residence time on the catalytic conversion of 4-NP by the Au@PmPD membrane was investigated by modulating the flow rate through the control of the external pressure, as shown in Fig. 7a. During the catalytic reduction process of 4-NP by the Au@PmPD membrane, a higher applied

pressure proportionally resulted in higher water flux, consequently shortening the contact time between 4-NP and the Au NPs within the catalytic membrane (Fig. S11†). This resulted in a discernible decrease in the catalytic conversion efficiency of 4-NP as the external pressure escalated from 0.2 to 2.6 bar, with efficiency diminishing from nearly 100% to about 82% once the pressure exceeded 2.0 bar.

Under each pressure, the residence time (R_t) of 4-NP within the membrane was calculated using $R_t = \frac{V_{eff}}{v}$, where V_{eff} is the effective pore volume of the Au@PmPD membrane and v is the flow rate of the solution. Detailed methodologies for measuring V_{eff} and calculating the flow rate at various applied pressures are described in Text S1 and depicted in Fig. S11.† The conversion of 4-NP was fitted using the first-order kinetics, and the reaction rate constant of 4-NP for the Au@PmPD membrane (k_{obs}) was determined to be 2.206 s^{-1} (Fig. 7b).

Fig. 7c presents a comparison of reductive conversion of 4-NP by the Au@PmPD membrane and other reported catalytic membranes focusing on the quantity of NaBH$_4$ added and the conversion rate constants. Remarkably, the Au@PmPD membrane showcased a significant efficiency in 4-NP reduction, requiring only 178.6 M of NaBH$_4$ to reduce 1 M of 4-NP. This was markedly lower than the amounts required in similar studies, such as the Cu-Ag-Au NPs@β-LGF membrane which

© 2024 The Author(s). Published by the Royal Society of Chemistry

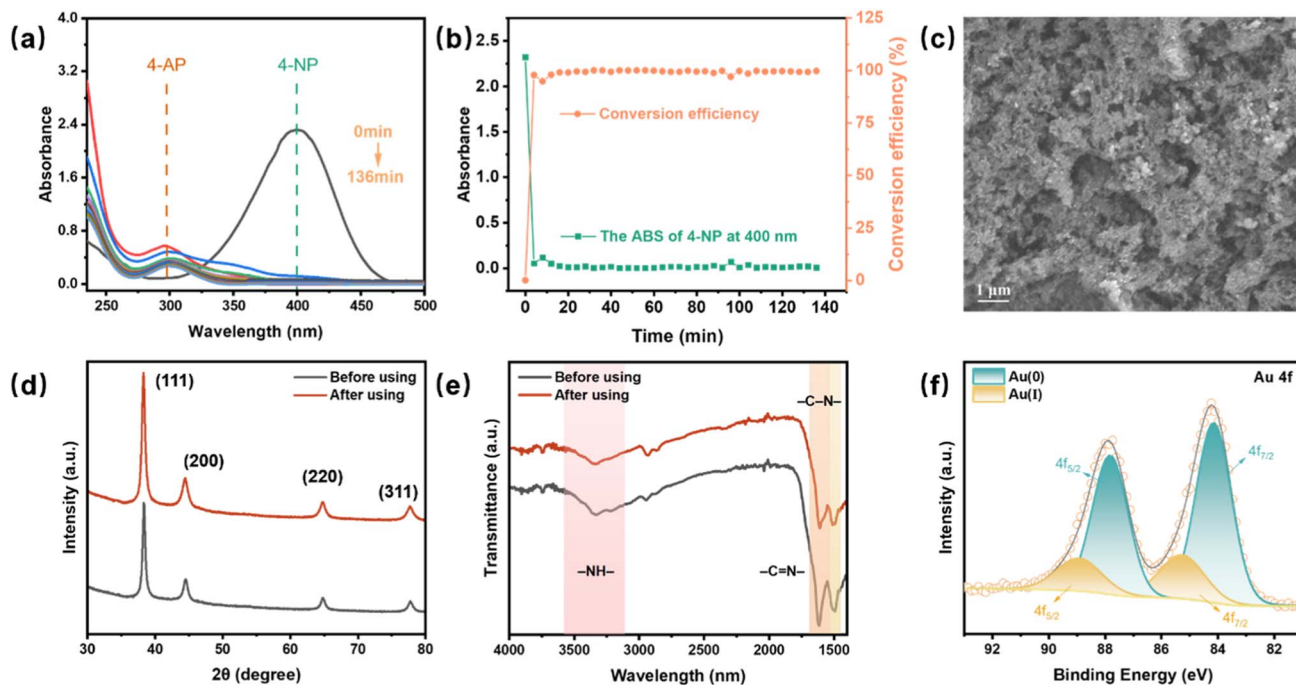Environ. Sci.: Adv., 2024, 3, 763–775 | 769

Fig. 6 The long-term catalytic performance of the Au@PmPD membrane in the conversion of 4-NP over a course of 136 min: (a) the time-resolved UV-vis spectra of the filtrate, (b) absorbance variations of 4-NP and the corresponding conversion ratio, (c) SEM image of the Au@PmPD membrane after a 136-min reaction, and the comparisons of (d) XRD pattern, (e) FT-IR spectra, and (f) Au 4f XPS spectra of Au@PmPD membranes before and after the 136-min reaction.

necessitated 1034.5 M of NaBH$_4$.[38] Moreover, compared to other studies that employed fewer amounts of NaBH$_4$, like the Ag/TiO$_2$/PVDF@TiO$_2$ membrane,[19] the Au@PmPD membrane not only achieved near 100% reductive conversion of 4-NP, but also exhibited a significantly higher reaction rate constant of 2.206 s^{-1}. Therefore, these results highlight the pivotal significance of the Au@PmPD membrane as an efficient catalytic membrane for the reductive conversion of 4-NP. The mechanism underlying the high catalytic activity is investigated below.

Mechanism for the enhanced catalytic activity

Nano-enabled catalytic membranes are typically prepared through impregnation or mixing methods. In the impregnation method, the membrane substrate is initially soaked in a solution containing the metal precursor, followed by reduction with a reducing agent to form metal nanoparticles. However, the mass loading of the precious metals is susceptible to the influence of solvent properties, soaking time, and substrate membrane properties. Moreover, the surface of the membrane substrate may be rapidly covered by the metal precursor. Once the surface is covered, further metal adsorption or deposition may be limited, resulting in limited mass loading and, subsequently, compromises catalytic efficiency. Conversely, the mixing method involves combining nanoparticles with the membrane material before membrane formation, resulting in a composite membrane with dispersed nanoparticles throughout the membrane matrix. This approach offers the advantage of achieving substantial and adjustable mass loading

of catalytic nanoparticles by precisely controlling the amounts of nanoparticles added.

To evaluate the efficacy of our *in situ* extraction and formation method *versus* the direct mixing method for Au incorporation, we prepared two types of gold-containing PmPD membranes using each method and assessed their conversion efficiency for 4-NP. Fig. 8a and b depict the schematic illustrations of the *in situ* extraction and formation method, as well as the direct physical mixing method. In the direct-mixing method, Au NPs with an average particle size of 32 nm (Fig. S12†), akin to those in Au@PmPD, were prepared by reducing 100 mL HAuCl$_4$ solution (10^{-2} wt%) with 1.0 mL sodium citrate (1 wt%).[44] Following thorough mixing of PmPD and Au NPs, the resultant mixture was vacuum-filtered on the nylon membrane substrate, ensuring the same PmPD and Au mass loadings in the membrane as in the typical Au@PmPD membrane. The comparative results, as shown in Fig. 8c and d, demonstrate a nearly complete conversion of 4-NP by our *in situ* formation membrane, whereas the directly mixed membrane exhibited only a 55.2% removal efficiency. This stark contrast highlights the superior performance and efficiency of the *in situ* extraction and formation method in catalyzing 4-NP conversion.

The notable difference in catalytic efficiency is largely due to the distinct distribution of Au NPs within the membrane matrix and, consequently, affecting the exposed surface area of catalytic Au NPs. Due to the agglomeration effect of Au NPs, the direct-mixing method leads to uneven dispersion of Au NPs throughout the PmPD membrane matrix. Moreover, owing to
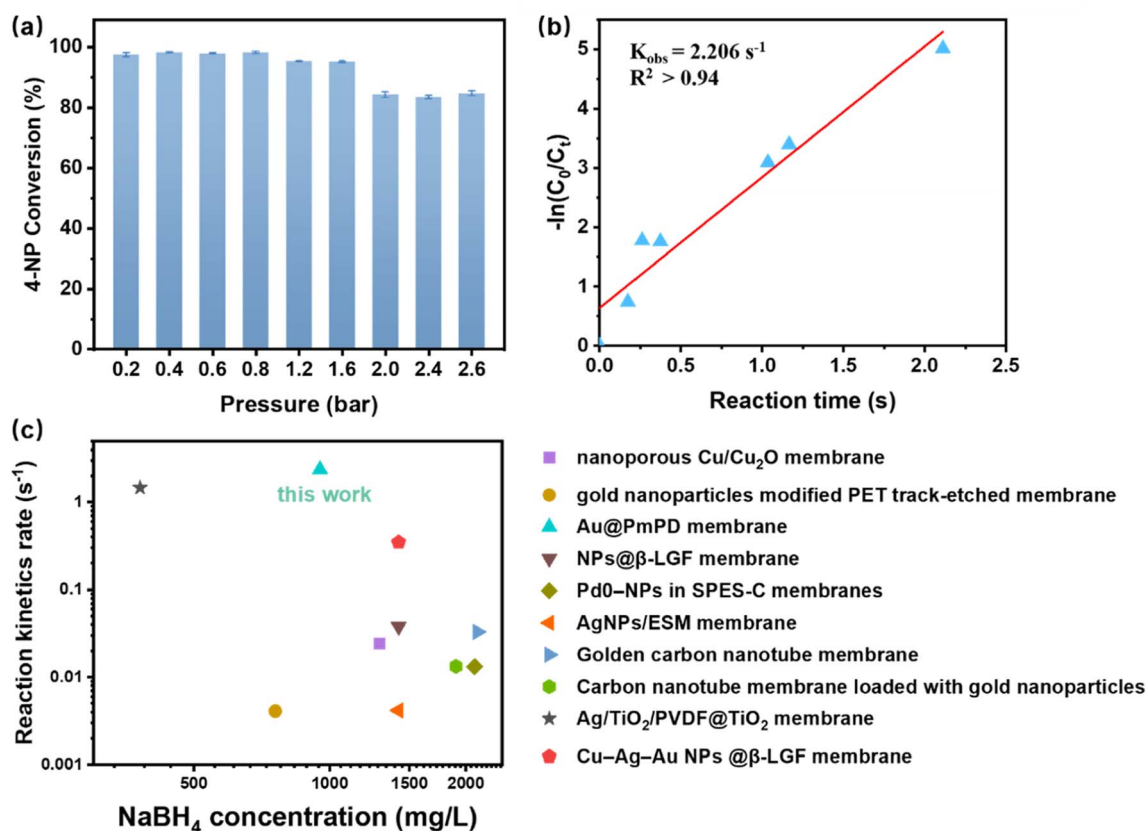
Fig. 7 The reaction kinetics of 4-NP reduction catalyzed by the Au@PmPD membrane: (a) 4-NP conversion under external pressure ranging from 0.2 to 2.6 bar, and (b) plot of $-\ln(C_0/C_t)$ versus reaction time for the catalytic reduction of 4-NP. (c) Comparison of the rate constants in the catalytic degradation of 4-NP by the Au@PmPD membrane with those by the membranes reported in the published literature.[19,36–43]

the embedding effect,[45] the exposed surface of Au NPs may be partially covered by the PmPD matrix, limiting the availability of active sites for catalytic reactions. In contrast, membranes created via in situ Au extraction and formation present several benefits. In this in situ method, Au(III) was reduced to Au NPs by PmPD, thus anchoring them to the PmPD membrane surface. This ensures a more uniform distribution on the surface of the PmPD membrane matrix, alleviating the embedding and agglomeration effects, thereby providing more catalytic sites on the membrane surface compared to its physically mixed counterparts, which contributes to enhanced catalytic activity. Moreover, the chemical bonds between Au NPs and the PmPD membrane lead to a stronger binding force, potentially increasing the stability and durability of the catalytic membrane during its application.

Practical application prospects

To assess the feasibility of recovering Au from actual electronic wastewater and employing it for the remediation of practical 4-NP-containing wastewater, a circuit board dissolved in aqua regia was utilized to represent the electronic wastewater derived from e-waste leached using aqua regia. The solution was highly acidic, with a pH value below zero. It was characterized by a wide range of metal ions at varying concentration levels.

Predominantly, the solution has a high concentration of Cu^{2+}, succeeded by considerable quantities of Fe^{3+}, Zn^{2+}, Al^{3+}, and Ni^{2+}, while Pb^{2+} and Au^{3+} were present at trace concentrations, demonstrating a complex challenge for Au recovery. Considering the prevalence of 4-NP in challenging dyeing wastewater, methylene blue (MB) dyeing wastewater, known for its high alkalinity and high salinity, was selected as a surrogate for the typical 4-NP-containing wastewater. Specifically, MB dyeing wastewater is characterized by its large volume, complex composition, and presence of dyes, leading to high COD and BOD levels, strong biotoxicity, and intense coloration. Notably, even at low concentrations, the MB wastewater exhibits significant staining, making its treatment challenging. The detailed characteristics of the water quality for both types of wastewater are provided in Tables S2 and S3.†

After utilizing a 15 mg PmPD membrane to extract Au from 10 mL of electronic wastewater, the outcomes (Fig. 9a) revealed that the PmPD membrane attained a 100% recovery rate of Au, effectively outperforming numerous other competing metal cations. The mechanism underlying this efficient recovery can be attributed to the affinity of the PmPD membrane's amino groups for Au. Specifically, Au exists as $AuCl_4^-$ in the electronic wastewater and is electrostatically attracted to the positively charged PmPD membrane, facilitating selective adsorption of
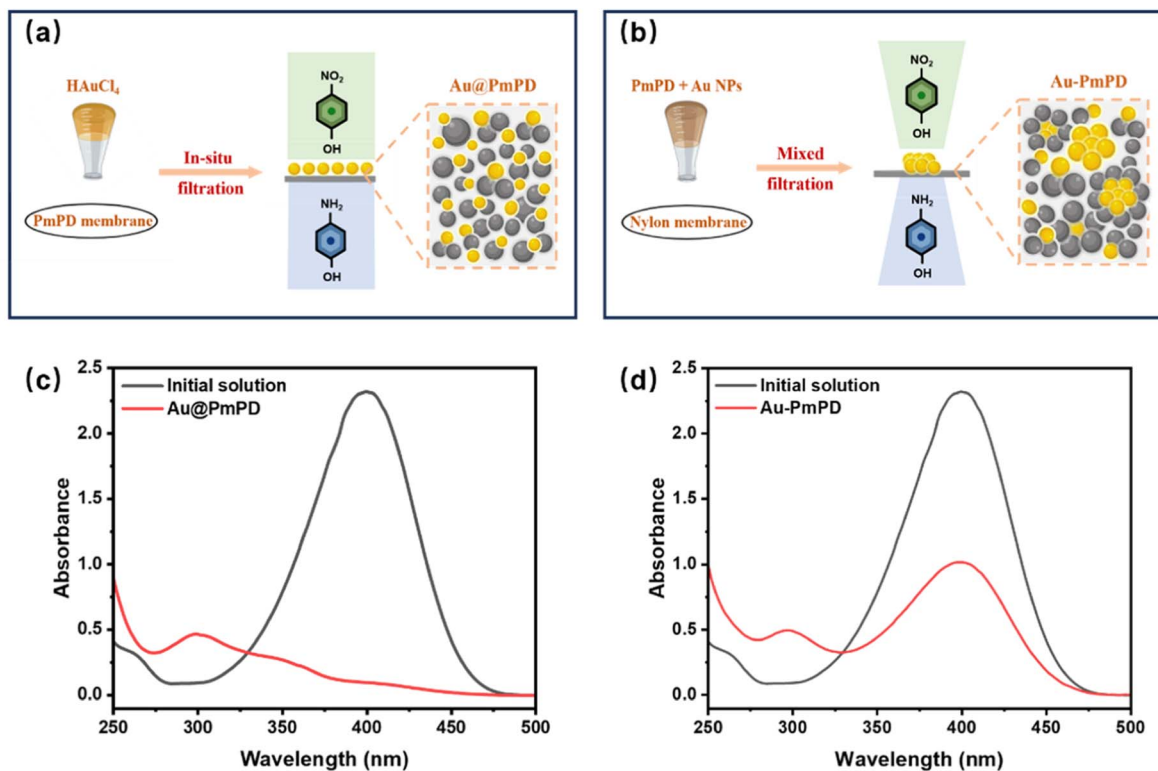
Fig. 8 Comparison of catalytic performance of the *in situ* membrane and direct mixing membrane: schematic illustrations of the formation and the resulting Au distribution pattern for (a) *in situ* Au@PmPD membrane and (b) a mixed Au-PmPD membrane and the UV-vis spectra of (c) Au@PmPD membrane filtrate and (d) Au-PmPD membrane filtrate. A 20 mg L^{-1} 4-NP solution was passed through both membranes in the single-pass mode without recirculation.
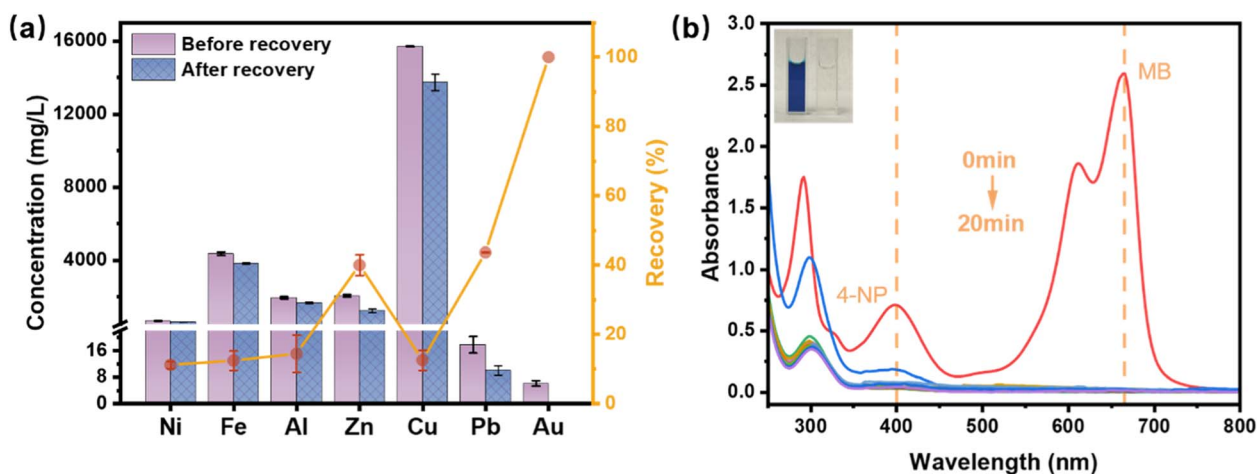

Fig. 9 Remediation performance for practical wastewater: (a) concentrations of metal cations in the electronic wastewater before and after treatment with the PmPD membrane, alongside the recovery efficiency for each metal; (b) changes in UV-vis absorbance for 4-NP and MB during the catalytic reduction reaction (note: the solution for the initial absorbance curve was diluted to one-fourth of its original concentration).

Au(III). Conversely, other cations are electrostatically repelled, which minimizes their interaction with the membrane. This underscores the PmPD membrane's superior proficiency in gold recovery from authentic electronic wastewater. Furthermore, as depicted in Fig. 9b, the reclaimed membrane showcased robust catalytic reduction performance, successfully eliminating 4-NP

and MB with an excess of NaBH$_4$ (0.1 M), where all samples post-1-minute treatment reached a 100% removal rate for both 4-NP and MB. Moreover, as the image inserted in Fig. 9b shows, the solution underwent a noticeable transition from a dark blue to complete colorlessness, indicating successful decolorization. This was attributed to the catalytic reduction, converting MB

into its colorless form, leuco-methylene blue, and 4-NP into 4-AP. Subsequent XRD patterns of the PmPD membranes, before and after the catalytic reaction, highlighted that among these metals detected, only characteristic peaks for Au were exhibited, and no significant changes were observed in the spectra, evidencing the PmPD membranes' exceptional selectivity for Au and their stability. Thus, the PmPD membrane not only excels in retrieving Au(III) from electronic wastewater but also serves as an efficient catalytic medium for 4-NP wastewater treatment, effectively converting waste into a valuable asset and mitigating environmental pollutants through waste conversion.

Conclusion

This study successfully demonstrated the potential of Au@PmPD membranes in addressing two significant environmental challenges: the recovery of gold from electronic waste and the catalytic reduction of nitrophenol in wastewater. The membranes, synthesized *via* an innovative *in situ* extraction and formation method, exhibited exceptional gold recovery capabilities, achieving 100% extraction efficiency even amidst competing metal cations. Moreover, the Au-laden membranes showcased remarkable catalytic efficiency in converting 4-NP to 4-AP, maintaining near 100% conversion efficiency under various operational conditions. The study also established the membrane's robustness, with stable catalytic performance over extended periods and minimal impact from co-existing anions and pH variations. The findings of this study underscore the feasibility of employing nano-enabled catalytic membranes obtained from resource recovery for environmental remediation. By transforming waste into valuable catalytic entities, this approach not only mitigates the environmental impact of pollutants but also contributes to resource sustainability, contributing to a circular economy model. Future investigations are crucial for exploring their performance in varied wastewater compositions, particularly regarding organic matter, which is essential for optimizing their applications in real-world scenarios.

Author contributions

YX: methodology, investigation, conceptualization, data analysis, visualization, writing – original draft; YC: methodology, investigation, data analysis, writing – original draft; MW: investigation, data analysis; YS: investigation, data analysis; SC: investigation, data analysis; ZW: conceptualization, funding acquisition, investigation, project administration, resources, writing – review and editing.

Conflicts of interest

The authors declare no conflicts of interest.

Acknowledgements

References

1 S. Payra, S. Challagulla, C. Chakraborty and S. Roy, A hydrogen evolution reaction induced unprecedentedly rapid electrocatalytic reduction of 4-nitrophenol over ZIF-67 compare to ZIF-8, *J. Electroanal. Chem.*, 2019, **853**, 113545.

2 Y. Yuan, B. Lai and Y. Tang, Combined Fe0/air and Fenton process for the treatment of dinitrodiazophenol (DDNP) industry wastewater, *Chem. Eng. J.*, 2016, **283**, 1514–1521.

3 Y. Li, W. Hsieh, R. Mahmudov, X. Wei and C. P. Huang, Combined ultrasound and Fenton (US-Fenton) process for the treatment of ammunition wastewater, *J. Hazard. Mater.*, 2013, **244–245**, 403–411.

4 B. Zhao, G. Mele, I. Pio, J. Li, L. Palmisano and G. Vasapollo, Degradation of 4-nitrophenol (4-NP) using Fe–TiO$_2$ as a heterogeneous photo-Fenton catalyst, *J. Hazard. Mater.*, 2010, **176**(1–3), 569–574.

5 Z. Xiong, H. Zhang, W. Zhang, B. Lai and G. Yao, Removal of nitrophenols and their derivatives by chemical redox: A review, *Chem. Eng. J.*, 2019, **359**, 13–31.

6 P. K. Arora, A. Srivastava and V. P. Singh, Bacterial degradation of nitrophenols and their derivatives, *J. Hazard. Mater.*, 2014, **266**, 42–59.

7 M. A. Rubio, E. Lissi, N. Herrera, V. Pérez and N. Fuentes, Phenol and nitrophenols in the air and dew waters of Santiago de Chile, *Chemosphere*, 2012, **86**(10), 1035–1039.

8 Y. Ji, Y. Shi, D. Kong and J. Lu, Degradation of roxarsone in a sulfate radical mediated oxidation process and formation of polynitrated by-products, *RSC Adv.*, 2016, **6**(85), 82040–82048.

9 B. Pan and B. Xing, in *Adsorption of organic compounds by engineered nanoparticles*, ed. B. Xing, C. D. Vecitis and N. Senesi, John Wiley & Sons, Inc, Hoboken, NJ, USA, 2016, pp. 160–181.

10 R. Amadelli, L. Samiolo, A. De Battisti and A. B. Velichenko, Electro-oxidation of Some Phenolic Compounds by Electrogenerated O$_3$ and by Direct Electrolysis at PbO$_2$ Anodes, *J. Electrochem. Soc.*, 2011, **158**(7), P87–P92.

11 T. K. Das and N. C. Das, Advances on catalytic reduction of 4-nitrophenol by nanostructured materials as benchmark reaction, *Int. Nano Lett.*, 2022, **12**(3), 223–242.

12 Z. Yan, L. Fu, X. Zuo and H. Yang, Green assembly of stable and uniform silver nanoparticles on 2D silica nanosheets for catalytic reduction of 4-nitrophenol, *Appl. Catal. B: Environ.*, 2018, **226**, 23–30.

13 C. Chen, L. Lu, L. Fei, J. Xu, B. Wang, B. Li, L. Shen and H. Lin, Membrane-catalysis integrated system for contaminants degradation and membrane fouling mitigation: A review, *Sci. Total Environ.*, 2023, **904**, 166220.

14 X. Liu, D. Xu, D. Zhang, G. Zhang and L. Zhang, Superior performance of 3 D Co-Ni bimetallic oxides for catalytic degradation of organic dye: Investigation on the effect of catalyst morphology and catalytic mechanism, *Appl. Catal. B: Environ.*, 2016, **186**, 193–203.

15 Y. Yu, Q. Zhang, M. Chi, H. Jiang, X. Liu, S. Wang and D. Min, Porous wood decorated with gold nanoparticles as flow-through membrane reactor for catalytic hydrogenation of methylene blue and 4-nitrophenol, *Cellulose*, 2021, **28**(11), 7283–7294.

16 X. Fang, J. Li, B. Ren, Y. Huang, D. Wang, Z. Liao, Q. Li, L. Wang and D. D. Dionysiou, Polymeric ultrafiltration membrane with *in situ* formed nano-silver within the inner pores for simultaneous separation and catalysis, *J. Membr. Sci.*, 2019, **579**, 190–198.

17 J. You, C. Shanmugam, Y. Liu, C. Yu and W. Tseng, Boosting catalytic activity of metal nanoparticles for 4-nitrophenol reduction: Modification of metal naoparticles with poly (diallyldimethylammonium chloride), *J. Hazard. Mater.*, 2017, **324**, 420–427.

18 M. T. Islam, R. Saenz-Arana, H. Wang, R. Bernal and J. C. Noveron, Green synthesis of gold, silver, platinum, and palladium nanoparticles reduced and stabilized by sodium rhodizonate and their catalytic reduction of 4-nitrophenol and methyl orange, *New J. Chem.*, 2018, **42**(8), 6472–6478.

19 Y. Wang, S. Ma, M. Huang, H. Yang, Z. Xu and Z. Xu, Ag NPs coated PVDF@TiO2 nanofiber membrane prepared by epitaxial growth on TiO2 inter-layer for 4-NP reduction application, *Sep. Purif. Technol.*, 2019, **227**, 115700.

20 Q. Zhang, X. Fan, H. Wang, S. Chen and X. Quan, Fabrication of Au/CNT hollow fiber membrane for 4-nitrophenol reduction, *RSC Adv.*, 2016, **6**(47), 41114–41121.

21 Y. Chen, S. Guan, H. Ge, X. Chen, Z. Xu, Y. Yue, H. Yamashita, H. Yu, H. Li and Z. Bian, Photocatalytic Dissolution of Precious Metals by TiO2 through Photogenerated Free Radicals, *Angew. Chem., Int. Ed.*, 2022, **61**(50), e202213640.

22 S. Gavriely, S. Richter and I. Zucker, Selective metal recovery by mucin: turning gold from wastewater into a peroxymonosulfate-activated catalyst, *Environ. Sci.: Nano*, 2024, DOI: **10.1039/d3en00699a**.

23 S. Naik and J. Satya Eswari, Electrical waste management: Recent advances challenges and future outlook, *Total Environ. Res. Themes*, 2022, **1–2**, 100002.

24 S. Jeon, M. Ito, C. B. Tabelin, R. Pongsumrankul, N. Kitajima, I. Park and N. Hiroyoshi, Gold recovery from shredder light fraction of E-waste recycling plant by flotation-ammonium thiosulfate leaching, *Waste Manage.*, 2018, **77**, 195–202.

25 W. Zhao, J. Xu, W. Fei, Z. Liu, W. He and G. Li, The reuse of electronic components from waste printed circuit boards: a critical review, *Environ. Sci.: Adv.*, 2023, **2**(2), 196–214.

26 S. Ilyas, R. R. Srivastava and H. Kim, Gold recovery from secondary waste of PCBs by electro-Cl2 leaching in brine solution and solvo-chemical separation with tri-butyl phosphate, *J. Clean. Prod.*, 2021, **295**, 126389.

27 M. Huy Do, G. Tien Nguyen, U. Dong Thach, Y. Lee and T. Huu Bui, Advances in hydrometallurgical approaches for gold recovery from E-waste: A comprehensive review and perspectives, *Miner. Eng.*, 2023, **191**, 107977.

28 Y. Chen, M. Xu, J. Wen, Y. Wan, Q. Zhao, X. Cao, Y. Ding, Z. L. Wang, H. Li and Z. Bian, Selective recovery of precious metals through photocatalysis, *Nat Sustainability*, 2021, **4**(7), 618–626.

29 H. Shang, Y. Chen, S. Guan, Y. Wang, J. Cao, X. Wang, H. Li and Z. Bian, Scalable and selective gold recovery from end-of-life electronics, *Nat. Chem. Eng.*, 2024, **1**(2), 170–179.

30 D. T. Sun, N. Gasilova, S. Yang, E. Oveisi and W. L. R. Queen, Selective Extraction of Trace Amounts of Gold from Complex Water Mixtures with a Metal–Organic Framework (MOF)/ Polymer Composite, *J. Am. Chem. Soc.*, 2018, **140**(48), 16697–16703.

31 X. Chen, S. Guan, J. Zhou, H. Shang, J. Zhang, F. Lv, H. Yu, H. Li and Z. Bian, Photocatalytic Free Radical-Controlled Synthesis of High-Performance Single-Atom Catalysts, *Angew. Chem., Int. Ed.*, 2023, **62**(45), e202312734.

32 J. Cao, Z. Xu, Y. Chen, S. Li, Y. Jiang, L. Bai, H. Yu, H. Li and Z. Bian, Tailoring the Asymmetric Structure of NH2-UiO-66 Metal-Organic Frameworks for Light-promoted Selective and Efficient Gold Extraction and Separation, *Angew. Chem., Int. Ed.*, 2023, **62**(18), e202302202.

33 L. Ren, E. Al Yousif, F. Xia, Y. Wang, L. Guo, Y. Tu, X. Zhang, J. Shao and Y. He, Novel electrospun TPU/PDMS/PMMA membrane for phenol separation from saline wastewater *via* membrane aromatic recovery system, *Sep. Purif. Technol.*, 2019, **212**, 21–29.

34 L. Zhang, H. Wang, W. Yu, Z. Su, L. Chai, J. Li and Y. Shi, Facile and large-scale synthesis of functional poly(*m*-phenylenediamine) nanoparticles by Cu2+-assisted method with superior ability for dye adsorption, *J. Mater. Chem.*, 2012, **22**(35), 18244.

35 Y. Chen, L. Wang, Y. Shu, Q. Han, B. Chen, M. Wang, X. Liu, D. Rehman, B. Liu, Z. Wang and J. Lienhard, Selective Recovery of Gold from E-Wastewater Using Poly-m-phenylenediamine Nanoparticles and Assembled Membranes, *ACS Appl. Eng. Mater.*, 2023, **1**(8), 2127–2136.

36 X. Bai, D. Chen, Y. Li, X. Yang, M. Zhang, T. Wang, X. Zhang, L. Zhang, Y. Fu, X. Qi and W. Qi, Two-dimensional MOF-derived nanoporous Cu/Cu2O networks as catalytic membrane reactor for the continuous reduction of p-nitrophenol, *J. Membr. Sci.*, 2019, **582**, 30–36.

37 R. Subair, B. P. Tripathi, P. Formanek, F. Simon, P. Uhlmann and M. Stamm, Polydopamine modified membranes with *in situ* synthesized gold nanoparticles for catalytic and environmental applications, *Chem. Eng. J.*, 2016, **295**, 358–369.

38 R. Huang, H. Zhu, R. Su, W. Qi and Z. He, Catalytic Membrane Reactor Immobilized with Alloy Nanoparticle-Loaded Protein Fibrils for Continuous Reduction of 4-Nitrophenol, *Environ. Sci. Technol.*, 2016, **50**(20), 11263–11273.

39 B. Domènech, M. Muñoz, D. N. Muraviev and J. Macanás, Catalytic membranes with palladium nanoparticles: From

tailored polymer to catalytic applications, *Catal. Today*, 2012, **193**(1), 158–164.

40 M. Liang, R. Su, W. Qi, Y. Yu, L. Wang and Z. He, Synthesis of well-dispersed Ag nanoparticles on eggshell membrane for catalytic reduction of 4-nitrophenol, *J. Mater. Sci.*, 2014, **49**(4), 1639–1647.

41 Y. Liu, Y. Zheng, B. Du, R. R. Nasaruddin, T. Chen and J. Xie, Golden Carbon Nanotube Membrane for Continuous Flow Catalysis, *Ind. Eng. Chem. Res.*, 2017, **56**(11), 2999–3007.

42 H. Wang, Z. Dong and C. Na, Hierarchical Carbon Nanotube Membrane-Supported Gold Nanoparticles for Rapid Catalytic Reduction of p-Nitrophenol, *ACS Sustain. Chem. Eng.*, 2013, **1**(7), 746–752.

43 R. Laxmi, N. Gupta, R. P. Behere, R. K. Layek and B. K. Kuila, Polymer nanocomposite membranes and their application for flow catalysis and photocatalytic degradation of organic pollutants, *Mater. Today Chem.*, 2021, **22**, 100600.

44 G. Frens, Controlled Nucleation for the Regulation of the Particle Size in Monodisperse Gold Suspensions, *Nat. Phys. Sci.*, 1973, **241**(105), 20–22.

45 J. Wang, Z. Wu, T. Li, J. Ye, L. Shen, Z. She and F. Liu, Catalytic PVDF membrane for continuous reduction and separation of p-nitrophenol and methylene blue in emulsified oil solution, *Chem. Eng. J.*, 2018, **334**, 579–586.

© 2024 The Author(s). Published by the Royal Society of Chemistry

Environ. Sci.: Adv., 2024, **3**, 763–775 | **775**